Hindawi
Journal of Nanomaterials
Volume 2018, Article ID 7127843, 13 pages
https://doi.org/10.1155/2018/7127843

Research Article

Preparation of Silver-Doped Alumina Spherical Beads with Antimicrobial Properties

José Hafid Roque-Ruiz,[1] Daniela Castillo-Ramírez,[1] Álvaro de Jesús Ruíz-Baltazar,[2] León Francisco Espinosa-Cristóbal,[1] and Simón Yobanny Reyes-López[1]

[1]*Instituto de Ciencias Biomédicas, Universidad Autónoma de Ciudad Juárez, Envolvente del PRONAF y Estocolmo s/n, Ciudad Juárez, Chih., 32300, Mexico*
[2]*CONACYT-Centro de Física Aplicada y Tecnología Avanzada, Universidad Nacional Autonoma de Mexico, Boulevard Juriquilla 3001, 76230 Santiago de Querétaro, QRO, Mexico*

Correspondence should be addressed to Simón Yobanny Reyes-López; simon.reyes@uacj.mx

Received 23 January 2018; Revised 26 May 2018; Accepted 31 May 2018; Published 27 June 2018

Academic Editor: Ilker S. Bayer

The synthesis of composites with antibacterial properties is of great interest for the development of new biomedical applications. The antimicrobial properties of silver have been verified against microorganisms such as bacteria, viruses, and fungi; interest in silver has been renewed, so several technologies are currently in development, especially in dental materials. The purpose of this work was to improve the parameters for producing silver-doped alumina spherical beads using sodium alginate as a sacrificial template. Alumina is a biocompatible and thermally stable ceramic, while silver was used for its bactericidal properties. The obtained spheres presented a mean diameter of 2 mm, with an irregular surface and intertwined particles after a sintering process. After electrodeposition, white spheres turned to a dark gray color, demonstrating the presence of silver nanoparticles and fractal silver dendrites on the surface. Spheres were characterized by SEM, FTIR, and XRD. Antimicrobial activity of the alumina-AgP spheres against *E. coli*, *S. aureus*, *K. pneumoniae*, and *S. mutans* was analyzed by turbidimetry. The specific antimicrobial activity of all the composites showed specific antibacterial effects, independently of the amount of silver deposited, probably due to the differences in the microbial cell wall structures. Therefore, antibacterial activity depends on microbiological and structural characteristics of each bacterium.

1. Introduction

The control of emergent antibiotic-resistant bacteria has become a serious public health problem. Novel and better antimicrobial agents are still being developed to control associated microorganisms. However, this still represents a great challenge for antimicrobial agents. The scientific community conducts research to constantly develop new bioactive compounds or composites with antibacterial properties. The investigations are looking towards developing new bioactive composites with silver at a nanometric scale [1, 2]. In the last years, nanotechnology manipulates matter at an atomic scale creating new composites with novel properties. The novel properties of nanoparticles of composites have been widely investigated for their use in medicine, cosmetics, environment, and technology [2]. Novel and better antimicrobial agents are still being developed to control associated microorganisms. However, this still represents a great challenge for antimicrobial agents.

Silver nanoparticles (AgNP) present a high surface area and important antimicrobial capacity. However, it is necessary to use a matrix as a support material to avoid their dispersion. High concentrations of silver are toxic for humans and other organisms. Silver (Ag) is the most abundant and least expensive precious metal and is used in chemical industry as a catalyst for alcohol, alkenes, and olefin oxidation. Silver is widely used in photography, fabrication of electrical wires, and minting and as an antibacterial agent. The latter use is known since ancient times, and it has been demonstrated that silver salts

prevent infection in burns and injuries. Due to its antibacterial properties, silver is used as a sterile coating for prosthesis and catheters [3–5].

AgNP are widely used in pharmaceutical and food industries for their bactericide and fungicide properties, and recently, the interest has increased because of the emergence of antibiotic-resistant strains. Previously, the risks of exposure to high concentration of silver inhibited its potential use. However, nanotechnology has improved the efficiency of silver as an antimicrobial agent, due to the preparation of particles with a higher surface area and less toxicity to human beings [4].

The antibacterial activity of silver is caused by the continuous release of ions [5, 6], and different studies demonstrate the enhanced properties of nanoparticles when compared to ionic compounds such as silver nitrate ($AgNO_3$) and silver chloride (AgCl) [7, 8]. The main advantage of AgNP over other morphologies is the high surface area for contact with media, enhancing antibacterial activity [9, 10]. Silver ions released through oxidation of nanoparticles interact and inhibit the activity of bacterial structures [5, 6]. Consequently, cell wall permeability increases and transport through the plasmatic membrane is affected, leading to cell death [7, 8]. Also, silver ions form insoluble compounds with sulfhydryl groups in enzymes, blocking the respiratory chain and DNA replication. Silver acts as an antimicrobial agent against a wide spectrum of Gram-negative and Gram-positive bacteria, including antibiotic-resistant strains. Recent studies demonstrate the potential use of nanometric silver materials against pathogens associated to biofilm formation, such as *Escherichia coli* (*E. coli*), *Streptococcus pneumoniae* (*S. pneumoniae*), *Staphylococcus aureus* (*S. aureus*), and *Aspergillus niger* (*A. niger*) [1, 9].

On the other hand, alumina is one of the most important ceramic materials used for industrial applications. Several alumina polymorphs have been used for the fabrication of catalysts and catalyst supports, adsorbent materials, and coatings. This ceramic presents high mechanical strength and hardness, as well as high thermal and corrosion resistance. Nanostructured ceramics possess enhanced mechanical properties such as strength and toughness, compared to monolithic materials [11, 12]. α-Alumina is a thermodynamically stable structure with oxygen atoms adopting hexagonal close packing with alumina ions filling two-thirds of the octahedral sites in the lattice. Ceramic spheres are widely used in a broad range of applications like catalysts or catalyst supports. Recently, the sol-gel dripping method together with sodium alginate proved to be an effective method to produce alumina beads having a desired size, shape, and microstructure [13].

Ceramic composites are being considered potential third generation orthopedic biomaterials in view of their facility to match the chemical, biological, and mechanical properties of the bone. The application of alumina in the medical field is still in the process and is expected a major role of metal oxide nanoparticles in this area. A few studies are available in the literature on the interaction of the alumina on bacterial species. The dental materials with silver have the objective of diminishing or preventing microbial colonization on the dental parts, promoting the arrest of caries and avoiding the formation of biofilms, increasing oral health. Therefore, changes in surface chemistry in ceramics are important in terms of microbial toxicity. The aim of this study was to obtain silver-doped alumina spheres (AgP-AS) with antibacterial properties. The structure, morphology, and optical properties of the obtained samples were systematically characterized by X-ray diffraction (XRD), scanning electron microscopy (SEM), and Fourier transform infrared (FT-IR). This study is focused on the results of complex antimicrobial studies. Also, in this paper, we report the minimal inhibitory concentration.

Table 1: Slurries used for preparing alumina spheres.

Slurry	Alumina (g)	PVA (g)	Sodium alginate (g)	Water (mL)
50 : 1	2.5	0.05	0.1	2.45
50 : 2	2.5	0.1	0.1	2.4
50 : 5	2.5	0.25	0.1	2.25
60 : 1	3	0.05	0.1	1.95
60 : 2	3	0.1	0.1	1.9
60 : 5	3	0.25	0.1	1.75
70 : 1	3.5	0.05	0.1	1.45
70 : 2	3.5	0.1	0.1	1.4

2. Materials and Methods

2.1. Preparation of Alumina Spheres and AgP-AS. The obtention of ceramic beads is using alginates as a template. This approach produces ceramic beads whit antimicrobial properties. Now, a simple and inexpensive approach to produce spherical beads is by using a syringe. The exchange of ions takes place when sodium alginate replaces their monovalent Na^+ ions for divalent Ca^{2+} ions to form a semirigid body. Therefore, PVA was used to join particles heterogeneously, causing the union between particles by capillary forces during drying [13].

Sodium alginate and PVA with concentrations of 10 and 7%, respectively, were used for preparing the gel precursor solution. The alumina, PVA, alginate, and water weight ratios used for preparing eight slurries are shown in Table 1. Alumina powder (60 wt%), PVA 7% (2 wt%), sodium alginate 10% (2 wt%), and distilled water (36 wt%) were stirred magnetically until a homogenous white slurry was obtained. This paste was loaded on a syringe (5 mL) and placed vertically over a beaker with gelling solution ($BaCL_2$ 0.6 M), with a distance of 2 cm. A steel needle with a 0.71 mm diameter was used. Then the slurry was added dropwise to form spheres. After aging for 1 day in the gelling solution, the spheres were dried at 100°C for 2 h. Thermal treatment was applied in two steps; first, spheres were placed in a muffle furnace at 800°C for 2 h, with a heating ramp of 5°C/min, and next, the material was sintered at 1600°C for 2 h, using the same ramp.

Once sintering concluded, the dense alumina spheres were doped with AgP by electrodeposition. An electrolytic cell with silver anode was employed, while the alumina

(a) (b)

Figure 1: Alumina spheres after sintered at 1600°C: (a) 50 : 1 and (b) 60 : 2.

Table 2: Initial and final mean diameter of alumina spheres and shrink percentage.

Sample/ slurry	Initial diameter (mm)	Final diameter (mm)	Shrink (%)
50 : 1	2.90	1.86	35.86
50 : 2	2.65	2.29	13.46
50 : 5	2.81	2.03	27.75
60 : 1	2.29	1.96	14.45
60 : 2	3.44	2.01	41.57
60 : 5	2.62	2.04	21.83
70 : 1	2.55	1.89	25.59
70 : 2	4.33	2.49	42.49

spheres acted as a cathode. Silver nitrate solution 10 mM was added to the cell, and the spheres were treated for three different lapses of 1, 5, and 10 min. Electrodeposition was carried out at 39 and 69 mV, for each lapse.

2.2. Characterization. Alumina spheres before and after silver electrodeposition were characterized by Fourier-transform infrared spectroscopy (Alpha Platinum Bruker Instrument). The morphologies of the alumina sphere before and after silver electrodeposition were observed with a scanning electron microscopy (SEM, JEOLJSM-6400) operated at 20 kV. Before observation, the scaffolds were coated with platinum using a sputter coating. Crystalline phases were determined by X-ray diffraction analysis (XRD, Bruker D8 advance equipment) with Cu Kα radiation (1540 nm), operating at 20 kV with a scan range from 5° to 80°. The bulk density and apparent porosity were measured by the Archimedes method according to ASTM designation C 373-88.

2.3. Antimicrobial Analysis. References strains of *Escherichia coli* (*E. coli*, ATCC 25922), *Streptococcus mutans* (*S. mutans*, ATCC 25175), *Staphylococcus aureus* (*S. aureus*, ATCC 29213), and *Klebsiella pneumoniae* (*K. pneumoniae*, ATCC13883) were employed in the experiments. All of them were incubated at 37°C for 24 h in test tubes with Bioxon broth (BD) culture media. After this time, 100 μL of each suspension was inoculated in 3 mL BD broth media. Finally, AgP-AS were added to each test tube, while noninoculated samples were used as a control. All test tubes were incubated at 37°C, and a UV-Vis spectrophotometer (Agilent 85439) was used to determine changes in optical density at 600 nm after 24 and 48 h according to McFarland standards. In general, the antimicrobial activity was determined through changes in the absorbance values from alumina spheres exposed and nonexposed to silver electrodeposition confirmed by independently comparison between alumina samples (Mann–Whitney U test). Experiments were conducted in triplicate.

2.4. Statistical Analysis. A one-way analysis of variance (95%) of the data obtained was carried out using the Minitab 17 software. Also, Tukey's test was used for mean separation, while box-plot graphics were employed for comparison between groups. All data were expressed as the mean ± standard deviation. Significant differences between AgP-AS samples and microorganism groups were analyzed by Mann Whitney U test for nonparametric values (StatView software, SAS Institute Inc., v5.0.1, Cary, NC, USA). Pearson's analysis was also used to determine significant correlations between the antimicrobial activity and the intensity of electrodeposition (IBM-SPSS software, v24). Samples were considered significantly different when $p < 0.05$.

3. Results and Discussion

3.1. Characterization of Alumina Spheres. Figure 1 shows an alumina sphere photo after thermal treatment taken with a 14-megapixel normal camera. Sintered spheres presented a slight irregular surface of faint beige coloration and a structure with high mechanical strength. Some spheres showed for relaxation 60 : 2 a ~2 mm of diameter and small cracks and protuberances. Shrink percentage and volume loss were determined from the mean diameters of alumina spheres before and after thermal treatment, as shown in Table 2.

Table 3: Physical properties of alumina spheres after the sintering process.

Sample/ slurry	Apparent porosity (%)	Water absorption (%)	Bulk density (g/cm^3)
50 : 1	34.77	17.56	1.99
50 : 2	42.70	22.48	1.90
50 : 5	52.58	35.37	1.59
60 : 1	44.52	23.87	1.87
60 : 2	45.70	22.11	1.75
60 : 5	58.38	39 : 27	1.48
70 : 1	40.11	21.55	1.85
70 : 2	47.09	18.50	2.17

The alumina spheres with the most regular round shape were obtained from the slurries prepared with 60% of ceramic (60 : 1, 60 : 2, and 60 : 5). This slurry allowed the formation of homogenous structures with no elongation. By contrast, slurries with lower or higher percentage of alumina resulted in defective shapes. For instance, slurries with 50% of alumina yielded drop-shaped spheres due to their lower viscosity, and dripping occurred faster. On the other hand, the slurries with 70% alumina were highly viscous compared to the preceding pastes. As a result, slurry could not drip properly through the needle, forming a thick thread instead. Slurry 60 : 2 was selected as the best ratio for preparing alumina spheres, for it is easy to conform into a material with highly regular morphology. Furthermore, this ratio presented a high shrink percentage.

Density, porosity, and water absorption percentage were determined by the Archimedes method. Mean values of the three properties are shown in Table 3. Spheres obtained from slurry 60 : 2 were selected as the best material for the electrodeposition process. Spheres obtained from this slurry show the adequate porosity, water absorption, and density values. As shown in Table 3, the highest PVA ratio caused increment in porosity. This effect was caused by the agglomerating properties of the polymer, which also aids the generation of pores. PVA causes the union between particles by capillary forces during drying. The higher porosity values are related to an increment in water absorption and lower densities. Furthermore, the low decomposition temperature of PVA (beginning at 280°C) was appropriate for the thermal treatments applied to the precursor spheres.

Figure 2 shows the microstructure by SEM analysis of alumina spheres obtained from slurry 60 : 2. Before thermal treatment, the spheres showed round, rectangular, and square particles, with diameters from 0.5 to 1 μm. After sintering, the spheres present an intertwined structure, and grain growth was observed. Particles with the highest size values in the range from 2 to 4 μm are shown in a red frame. Porosity decreased because of the sintering process.

Figure 3 shows that alumina spheres obtained from slurry 60 : 2 acquired a light grayish coloration through silver electrodeposition. The particles exposed to the highest voltage (69 mV) for 10 min presents darker stains, because of the deposition of silver nanoparticles. Therefore, silver electrodeposition on the ceramic spheres depends on the exposition time to the highest voltage, as shown by the progressive increase in gray coloration from Figure 3(a) (39 mV for 1 min) to Figure 3(f) (69 mV for 10 min).

3.2. Characterization of AgP-AS. SEM micrographs of AgP-AS obtained from slurry 60 : 2 are shown in Figures 4 and 5. AgP with diameters ranging from 100 ± 80 nm were deposited on the alumina spheres treated at 39 mV (Figure 4(b)). Figure 4(c) shows a silver cluster with a diameter around 620 ± 70 nm. The nanoparticles are distributed irregularly on the surface and present different morphologies, mainly round and square shapes. Figure 5 shows SEM images from alumina spheres treated at 69 mV. At this voltage, a greater electrodeposition was achieved, compared to spheres treated at 39 mV and the nanoparticles still have the same size. Similarly, AgP (white area) were distributed unevenly on the sphere surface, forming small accumulations (agglomerates) on areas. In Figure 5(b), a silver dendrite-like growth is observed with a diameter of 5.5 μm and length around 9 μm. Silver dendrites present two and three-dimensional structures with only one stem (long axis) and several branches (short axes), which are like the work reported by Rezae and Damiri [14]. Nanobranches grew parallel to each other along *C*-axis, with a 60° angle to the stem. Dendritic growth is caused by a nucleation process; in this case, the growth is observed from particles of 100 nm, where the nanoparticles of Ag are deposited in thin sheets in a dendritic form. Consequently, dendrite length increases with longer electrodeposition time.

To support the results observed on SEM analysis and the significant antibacterial effects of the composite (Al_2O_3-Ag), a fractal Ag microdendrite model (QUANTA, Accelrys, San Diego, CA, USA) is presented in Figure 6. The figure shows the growth of the dendritic structure along the direction <110> of the Ag nanoparticles. The dendritic growth can be explained from the thermodynamics and crystallographic points of view. Thermodynamically, the Ag dendritic growth can be associated firstly to the Ag accumulation on the Al_2O_3 surface and secondly due to the temperature difference between the Al_2O_3 surface and the Ag. It is well known that the growing direction of these dendritic trunks is close to the thermal gradient direction. Several reports indicate that these factors can generate appropriate conditions for the dendritic solidification.

On the other hand, the Ag dendritic growth can be explained by the first-principle quantum-mechanical calculations. Based on the density functional theory, some modeling results of silver nanoparticles have been reported, which show that the binding energies of (110), (100), and (111) planes are 0.47, 0.29, and 0.27 eV, respectively. In this sense, it has been affirmed that the main dendritic growing is carried out along the <110> direction, due to its direction which exhibits major binding energy. Also, the Al_2O_3 surface promotes the nucleation and growth of the Ag nanoparticles and posterior fractal microdendrite Ag formation; this growth can be associated to the energy added during the electrodeposition process on the doped de Al_2O_3 spheres. As

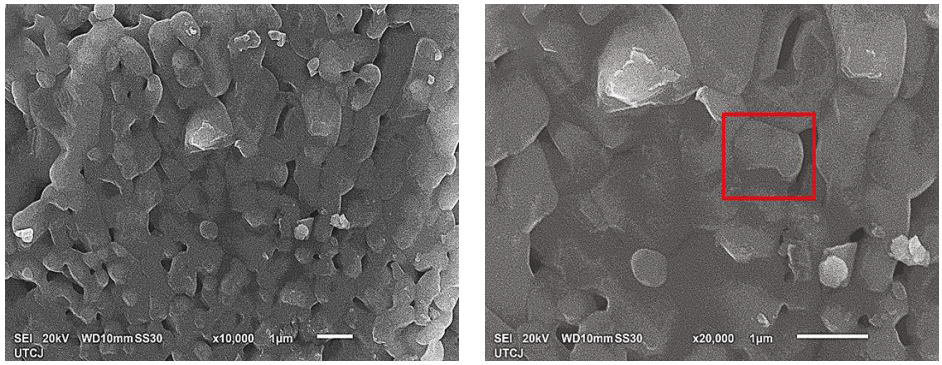

(a) (b)

Figure 2: Sintered alumina sphere at 1600°C observed by SEM at (a) 10,000x and (b) 20,000x.

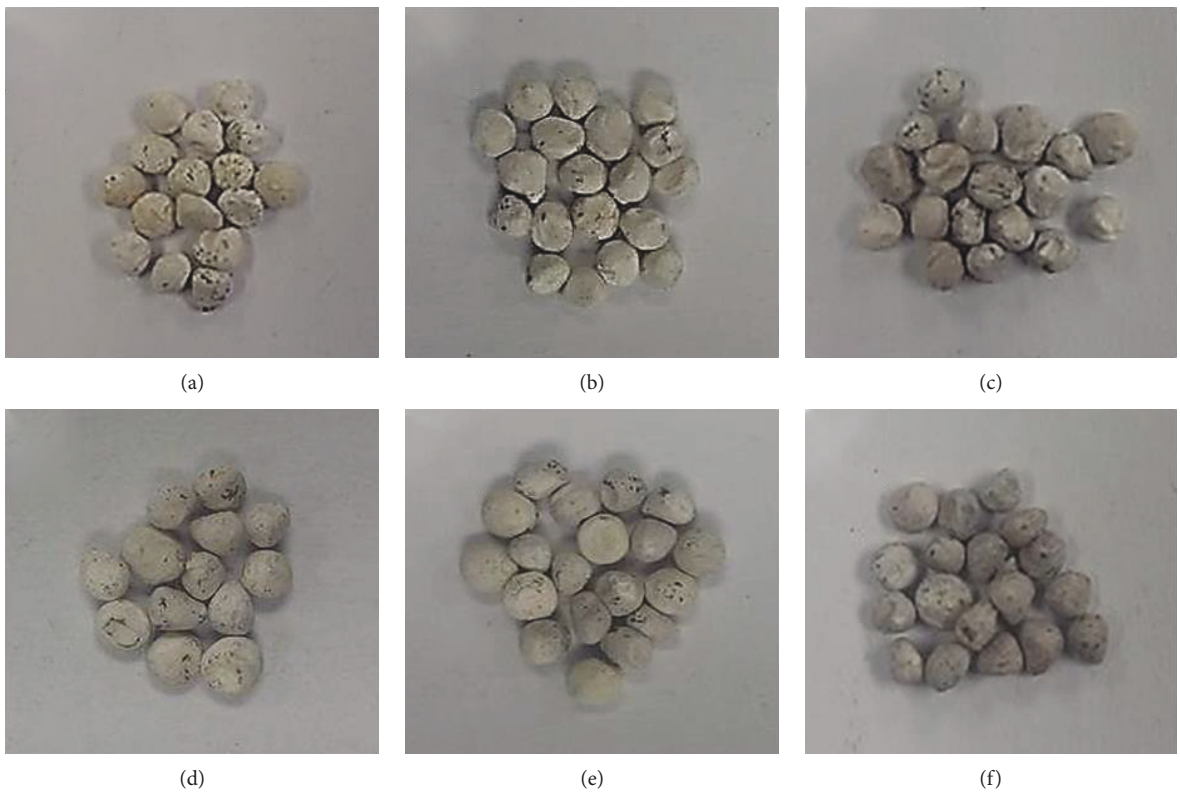

(a) (b) (c)

(d) (e) (f)

Figure 3: Alumina spheres doped with AgP by electrodeposition. Voltage 39 mV applied for (a) 1 min, (b) 5 min, and (c) 10 min. Voltage 69 mV applied for (d) 1 min, (e) 5 min, and (f) 10 min.

seen, the reactive sites and the voltage employed during the doping process promote the dendritic growth.

Infrared spectra and diffractogram from an XRD analysis of the sintered ceramic material at 1600°C after electrodeposition were obtained. Figure 7(a) represents the spheres doped at 69 mV for 5 min; the strong and well-defined IR bands observed for Al–O bonds must be explained considering the pure XRD refraction of α-alumina observed. A wide band between 500 and 1000 cm^{-1} corresponds to O-Al-O coordinated bonds. In the case of a corundum structure, it is built up only on octahedral AlO_6 and the most characteristic IR feature is the occurrence of two strong bands near 635, 565, and 491 cm^{-1} together with some other bands of less intensity around 450 and 780 cm^{-1}. This arrangement of aluminum and oxygen atoms denotes the formation of α-Al_2O_3 according to previous reports [11, 12]. The interaction between AgNP and alumina spheres was not observed in the infrared spectra. This aspect is important to achieve the antimicrobial function. The intensity of vibration bands corresponding to AgNP-AS increased due to the amount of sample analyzed.

The large enhancement of the vibrational mode indicates adsorption of energy onto the Ag particle. The ATR-FTIR spectroscopy consists of the passage of a beam

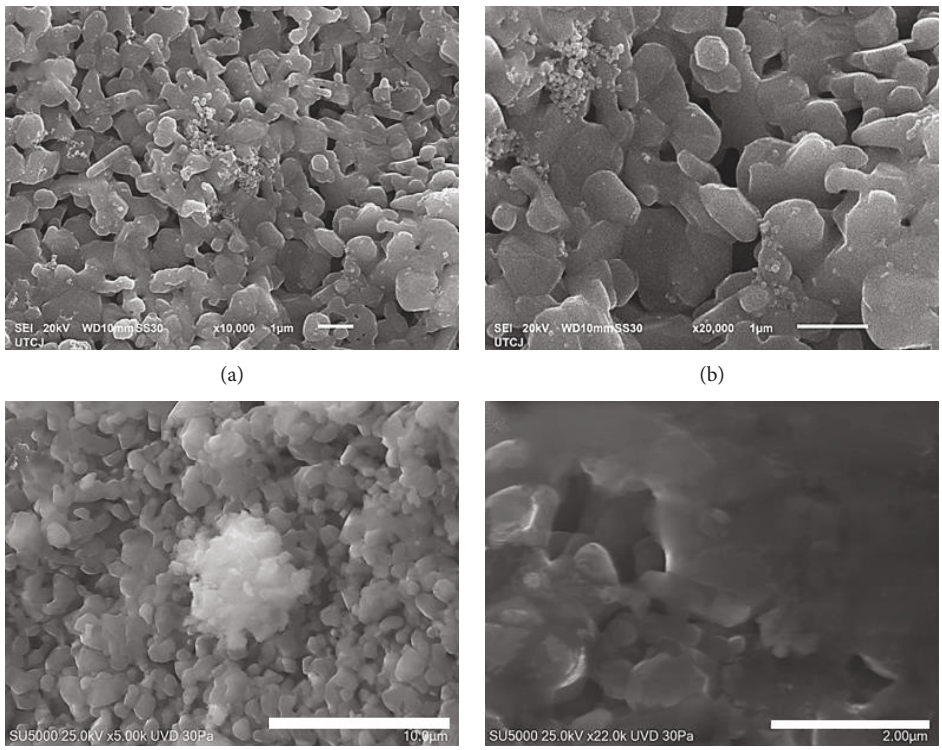

(a) (b)

(c) (d)

Figure 4: SEM images of AgP-AS treated at 39 mV during 1 min (a) 10,000x and (b) 20,000x and during 5 min (c) 5000x and (d) 22,000x.

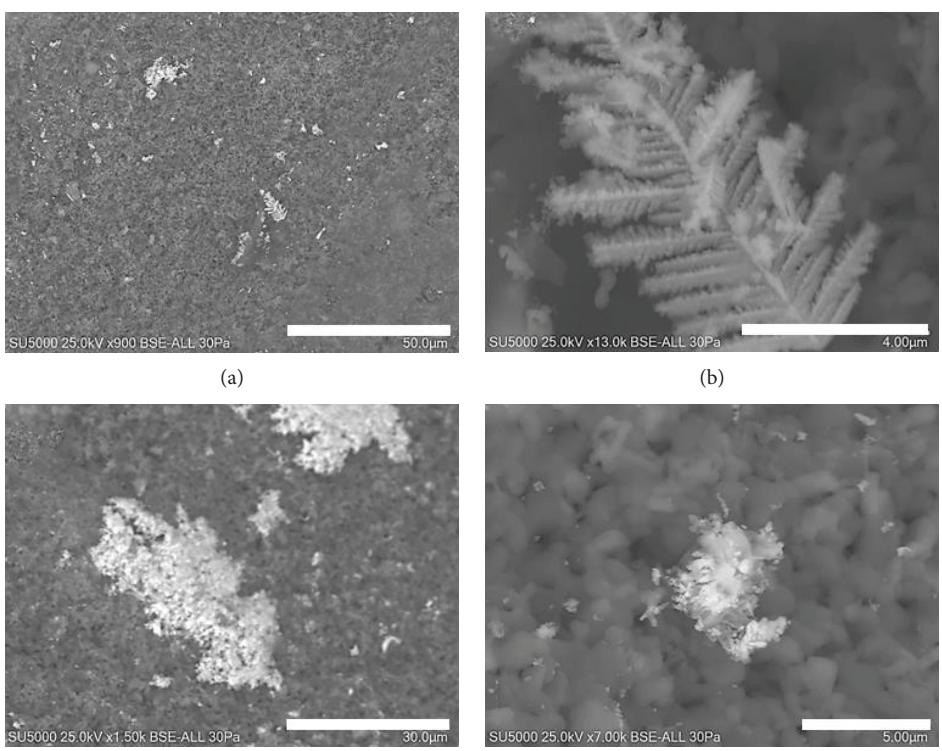

(a) (b)

(c) (d)

Figure 5: SEM images of AgP-AS treated at 69 mV during 1 min (a) 900x and (b) 13,000x and during 5 min (c) 1500x and (d) 7000x.

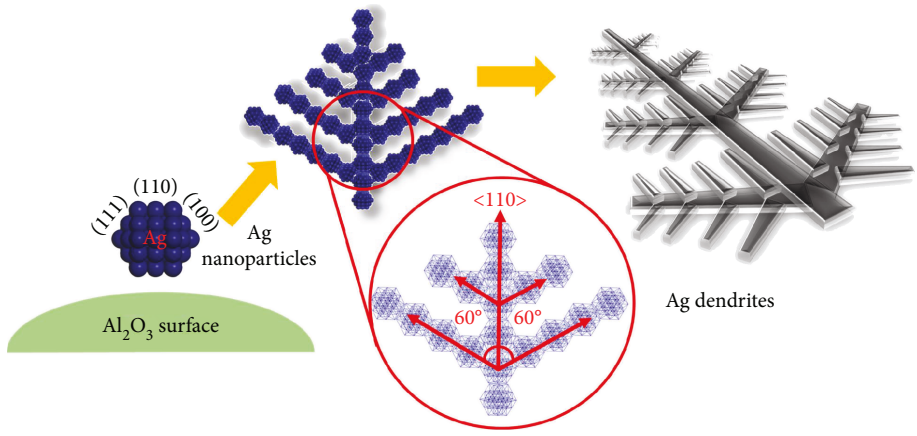

Figure 6: Scheme of the Ag dendritic growth from the Ag nanoparticles on the Al_2O_3 surface by electrodeposition.

of infrared radiation through a crystal transparent to the IR and of high refractive index, on where the sample is placed. The incident IR beam is reflected several times, and the surface of the sample absorbs part of the radiation at characteristic frequencies. On the other hand, surface resonance plasmon occurs when a polarized light is directed from a prism with a high refractive index to a metal layer with a lower refractive index. This explains why amplification occurred in the intensity of the alumina bands. Each time the IR beam was reflected, it influenced the analyte, activating the resonance plasmon. Thus, the alumina absorbs the energy released by this process, increasing the amplitude of the vibrational movements of its bonds. The characteristic crystalline planes of α-alumina phase are observed in Figure 7(b), according to the card JCPDS 10-0173. This alumina polymorph is of great importance because of its hardness and stability. In the same way, the intensity of alumina peaks increased in the samples doped with AgNP.

Diffraction is an elastic scattering phenomenon occurring when a plane wave interacts with an obstacle or a slit having a size comparable to its wavelength. The intensity of a diffraction signal depends on the scattering power of the material. The maximum intensity of the peak is related to the breadth of the peak which, in turn, is inversely related to the size of the scattering domains. The scattered spherical wave has the same wavelength as the original one. Varying the 367 size of the obstacle or slit, or their number, the same wave will be diffracted in different ways, because of different interference effects. Therefore, the interaction of silver gives an increase on the intensity of the diffraction patterns.

3.3. Antimicrobial Activity. Table 4 and Figure 8 show the results of the antimicrobial activity of AgP-AS treated with different times and levels of electrodeposition. Figures 8(a) and 8(b) show results between *S. mutans* strain added with AgP-AS treated at 39 and 69 mV during 1, 5, and 10 min (denoted SM39-01, SM39-05, and SM39-10, resp.). Optical density was quantified by the dilution method for the evaluation of antimicrobial activity of AgP-AS treated at 39 and 69 mV for several times on *S. mutans* cultures. Pure alumina spheres were used as control, denoted with the label CSM (control *S. mutans*). Figure 8(a) shows a minimal inhibition by the AgP-AS against the bacterial cultures according to the control observing higher and significant inhibition values for spheres treated at 39 mV for 5 min (SM39-05) compared to the control group ($p < 0.05$). Figure 8(b) shows very similar results, in which the highest inhibition values were significantly achieved with spheres treated at 69 mV for 1 min (SM69-01) than the control group ($p < 0.05$). Also, the inhibition activity using spheres treated at 39 and 69 mV was slightly decreasing with the electrodeposition time observing an improved bacterial inhibition on *S. mutans* strain in a period of time shorter (Table 4). Scientific reports have considered to the *S. mutans* as the principal oral microorganism involved in the beginning and development of dental caries [15], but other systemic and heart disorders have also been associated [16]. Our results confirm the antibacterial activity of silver on the surface of AS against *S. mutans* bacteria. These results assume that the bacterial activity of AgP-AS could be associated with the size of Ag particles deposited on the surface of AS due to shorter lapses of electrodeposition (1 min) than larger periods (10 min). It is probable that the increasing bacterial growth inhibition on *S. mutans* strain was created by smaller Ag particles on the AS samples. These results agree with reported works that have also demonstrated the effectiveness of Ag particles against *S. mutans*, increasing the antibacterial activity with smaller particles [17–19].

Figures 8(c) and 8(d) show a comparison between *S. aureus* strains added with AgP-AS treated at 39 and 69 mV for 1, 5, and 10 min (denoted SA39-01, SA39-05, SA39-10, SA69-01, SA69-05, and SA69-10, resp.). It was determined that the increase in electrodeposition time did not enhance bacterial inhibition (Table 4); the optical density shows approximately the same values. The highest inhibition values for both spheres doped at 39 mV and 69 mV which were achieved with samples treated for 10 min (SA39-10 and SA69-10), as shown in Figures 8(c) and 8(d), respectively (Table 4). Both AgP-AS samples presented more remarkable statistical differences than the control group ($p \leq 0.001$). Our results indicate that AgP-AS might inhibit the bacterial growth even of microorganisms considered a public health problem, such as *S. aureus* [20]. Actually, *S. aureus* is

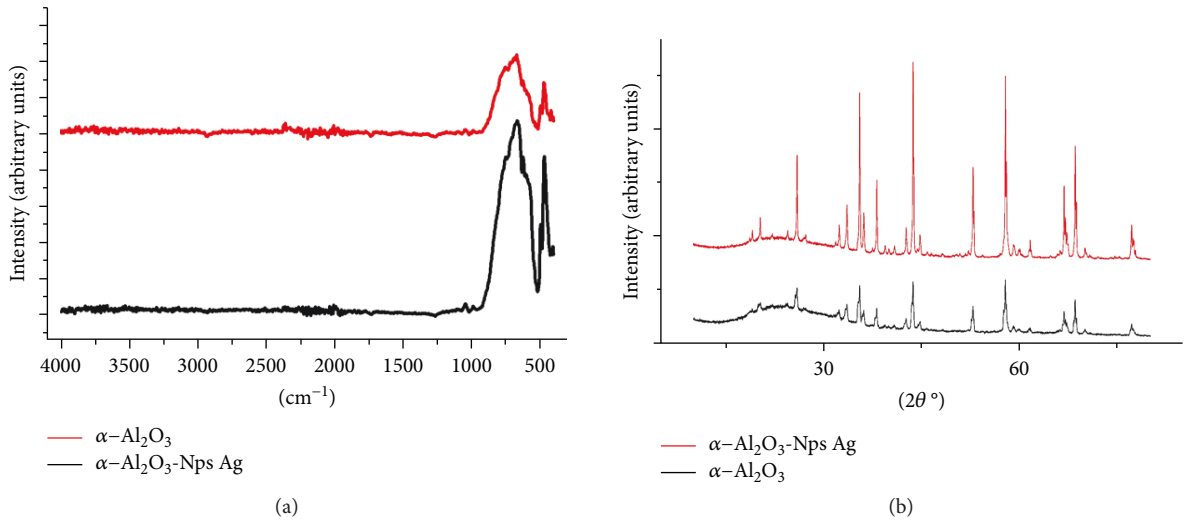

Figure 7: (a) Infrared spectra of sintered alumina and AgP-AS spheres at 1600°C and (b) XRD of alumina and AgP-AS.

considered one of the most important drug-resistant microorganisms related to infections acquired from health institutions producing skin and soft tissue infections, endocarditis, septicemia, and others [21]. Previous studies reported that Gram-positive bacteria, such as *S. aureus*, are more resistant to silver ions than Gram-negative bacteria [9, 18, 19]. These bacteria resist exposures to silver ions due to their cell wall with a thick peptidoglycan layer composed of teichoic acids, which limits the uptake of AgP [17, 18, 22].

Figures 8(e) and 8(f) show a comparison between *K. pneumoniae* strains added with AgP-AS treated at 39 and 69 mV for 1, 5, and 10 min (denoted KP39-01, KP39-05, KP39-10, KP69-01, KP69-05, and KP69-10, resp.). Inhibition of *K. pneumonia* by the ceramic composite was not observed in samples added with spheres treated at both voltages for 1 min (KP39-01 and KP69-01), and no significant difference was observed ($p > 0.05$). However, the increase in electrodeposition time enhanced bacterial inhibition showing statistically smaller values of optical density in groups treated with 10 min compared to the control group ($p < 0.05$). Also, the highest inhibition values for both doped spheres at 39 mV and 69 mV were significantly achieved with samples treated for 10 min in samples KP39-10 and KP69-10 ($p < 0.05$). This microorganism obtained opposite parameters according to the electrodeposition time where longer lapses of electrodeposition reduced considerably more bacteria than shorter periods. It means larger Ag particles deposited on the surface of spheres had more antimicrobial activity compared to smaller particles. *Klebsiella pneumoniae* is one of the major pathogens associated with nosocomial and community-acquired and resistant infections such as pneumonia, urinary tract infection (UTI), burn wounds, and septicemia [23]. One study evaluated chemically synthesized amino acid functionalized silver nanoparticles with gentamicin to eradicate *Klebsiella pneumoniae* biofilm. Results indicated that those particles demonstrated to have the potential application in the eradication of young and old *K. pneumoniae* biofilms [24]; however, therapeutic variations should be investigated.

Figures 8(g) and 8(h) show a comparison between *E. coli* strains added with AgP-AS treated at 39 and 69 mV for 1, 5, and 10 min. A wide range of bacterial inhibition activity was observed and was strongly achieved with spheres treated at 39 mV and 69 mV for 5 min (EC39-05 and EC69-05) than the control group with remarkable statistical differences ($p \leq 0.001$). Also, the inhibition activity of AgP-AS was not related with the increase of the electrodeposition time ($p > 0.05$). *E. coli* is a Gram-negative bacterium, with a cell wall consisting of an inner thin peptidoglycan layer and an outer layer of liposaccharides. The scarce thickness of the cell wall increases the susceptibility of these bacteria to silver ions released by nanoparticles on the composite [1]. Previous works with *E. coli* strains have reported that AgP can easily cross through the membrane and interact with protein synthesis, causing structural changes and death [1, 2].

Figure 9 shows bacterial growth inhibition results of AgP-alumina spheres treated at 24 and 48 h. For AgP-AS treated at 24 h (Figures 8(a)–8(h)), 39 and 69 mV samples showed to have significant bacterial growth inhibition for *S. mutans*, *S. aureus*, and *E. coli* compared to the control group ($p < 0.05$ and< 0.01); however, no statistical difference was demonstrated for *K. pneumoniae* strain ($p > 0.05$). Furthermore, the most resistant microorganism to AgP-AS samples treated at 24 h was *K. pneumoniae*, followed by *S. aureus* and *S. mutans*; the most sensitive strain was *E. coli* ($p < 0.01$) (Figures 8(e) and 8(f)). For AgP-AS treated at 48 h (Figure 9(c)), *S. aureus* and *E. coli* strains showed similar results than the 24 h group resulting in statistical differences of 39 and 69 mV samples compared to the control group ($p < 0.05$ and< 0.01). *S. mutans* and *K. pneumoniae* strains demonstrated to have similar bacterial growth than the control group, even when

Table 4: Antimicrobial activity of AgP-AS.

Strains	10^8 CFU/mL					
	0 mV		39 mV		69 mV	
	24 h	48 h	24 h	48 h	24 h	48 h
S. mutans	2.0 ± 0.1	2.0 ± 0.1	$1.7 \pm 0.1^{*}$	$1.9 \pm 2.6^{\dagger}$	$1.9 \pm 2.6^{*}$	2.0 ± 2.6
S. aureus	8.2 ± 0.0	$7.5 \pm 0.1^{\dagger}$	$4.9 \pm 0.2^{*}$	$4.0 \pm 0.2^{*\dagger}$	$5.0 \pm 0.4^{*}$	$4.2 \pm 0.3^{*\dagger}$
K. pneumoniae	10.2 ± 0.1	10.6 ± 0.1	10.2 ± 2.0	11.8 ± 2.3	11.1 ± 1.7	12.1 ± 1.7
E. coli	3.4 ± 0.1	$4.6 \pm 0.0^{\dagger}$	$0.7 \pm 0.3^{*}$	$3.4 \pm 3.8^{\dagger}$	$0.9 \pm 0.8^{*}$	$1.4 \pm 0.8^{*\dagger}$

All values are expressed in average and standard deviation in colony-forming units per milliliter (CFU/mL). *Statistical differences with the 0 mV group using similar times. †Statistical differences for each AgP-AS sample according to the time ($p < 0.05$).

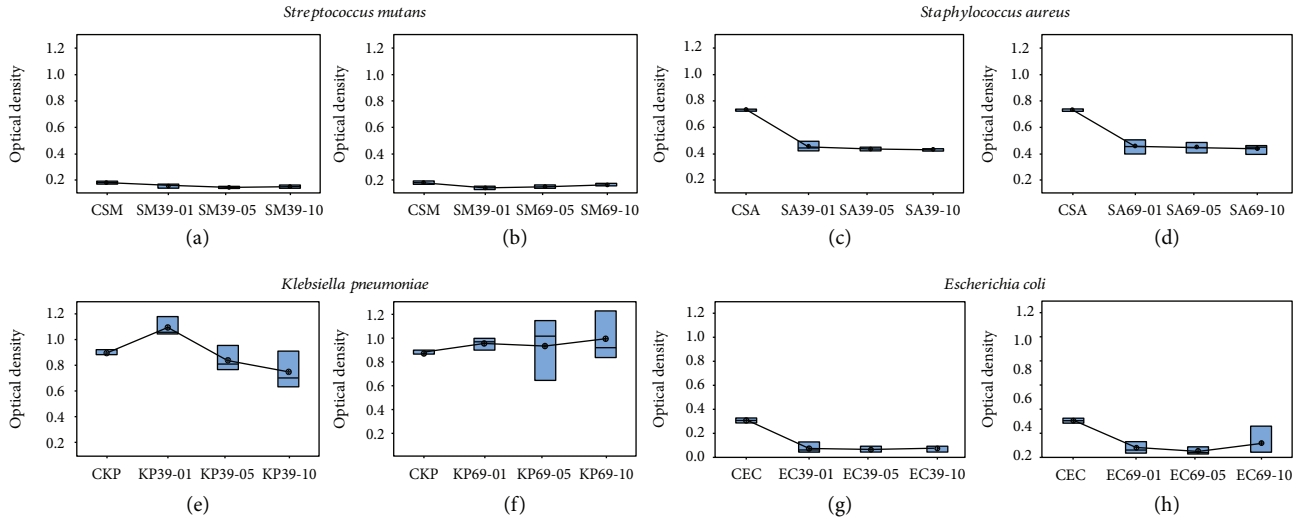

Figure 8: Box-plot graphics of bacteria strain cultures added with AgP-AS. (a, c, e, g) 39 mV and (b, d, f, h) 69 mV for 1, 5, and 10 min.

high voltages were used ($p > 0.05$). Additionally, the most resistant bacterial strain for AgP-AS treated at 48 h was *K. pneumoniae*, followed by *S. aureus* ($p < 0.01$); however, the most sensitive strains were *S. mutans* and *E. coli* ($p > 0.01$) (Figure 9(d)). These results suggest that the voltage and the type of microorganism play an important role in the antimicrobial capacity of AgP-AS samples. This association of bactericidal activity according to specific bacterial strains could be influenced by microbiological characteristics of each species, although physical and chemical properties of AgP-AS might also be involved [22].

On the other hand, bivariate Pearson's correlation analysis was used to determine significant correlations between antimicrobial activity and the intensity of electrodeposition. Significant positive and negative correlations were found for *S. aureus* (Pearson's correlation = 0.752, $p = 0.001$) and *E. coli* (Pearson's correlation = −0.420, $p = 0.006$) strains, respectively (Figures 10(b) and 10(d)), while *S. mutans* (Pearson's correlation = 0.012, $p = 0.941$) and *K. pneumoniae* (Pearson's correlation = 0.229, $p = 0.144$) showed no significant correlations (Figures 10(a) and 10(c)). In general, no significant correlations were found for all evaluated bacterial strains (Pearson's correlation = 0.023, $p = 0.768$) (Figure 10(e)).

In this study, the Gram-negative bacteria revealed the highest microbial resistance to AgP-AS; however, *E. coli* strain can also offer more antimicrobial inhibitory resistance than *S. aureus* strain to similar conditions [25]. Statistical analysis (Mann–Whitney *U* test) demonstrated that bacterial inhibition is directly related to the Ag concentration. However, significant and nonsignificant correlations derived from Pearson's analysis were also found; it could be explained by a specific response of each bacterium dependent on their metabolic characteristics as well as specific microbiological susceptibilities or resistance characteristics from the tested strains. *E. coli* and *K. pneumoniae* are Gram-negative bacteria, and their membranes present negative electrostatic charges, which attract and facilitate diffusion of AgNPs. The mechanism of antibacterial action by Ag nanoparticles is not understood accurately. However, previous studies have demonstrated the crucial role of electrostatic attraction between bacterial cells (negative) and nanoparticles (positive) [2].

It is well known that the size of AgNP is associated with low periods and intensities of voltages. This property has played an important role for antimicrobial activity in various microorganisms (smaller AgNP promotes better antimicrobial effect than larger particles); but also, ion release capacity, presence of coatings, zeta potential and other physical and chemical properties could be involved [18, 19, 22, 26, 27]. Regarding zeta potential, it is commonly used to determine the stability of nanoparticles in aqueous media determining the electrical charge and the attraction or repulsion of

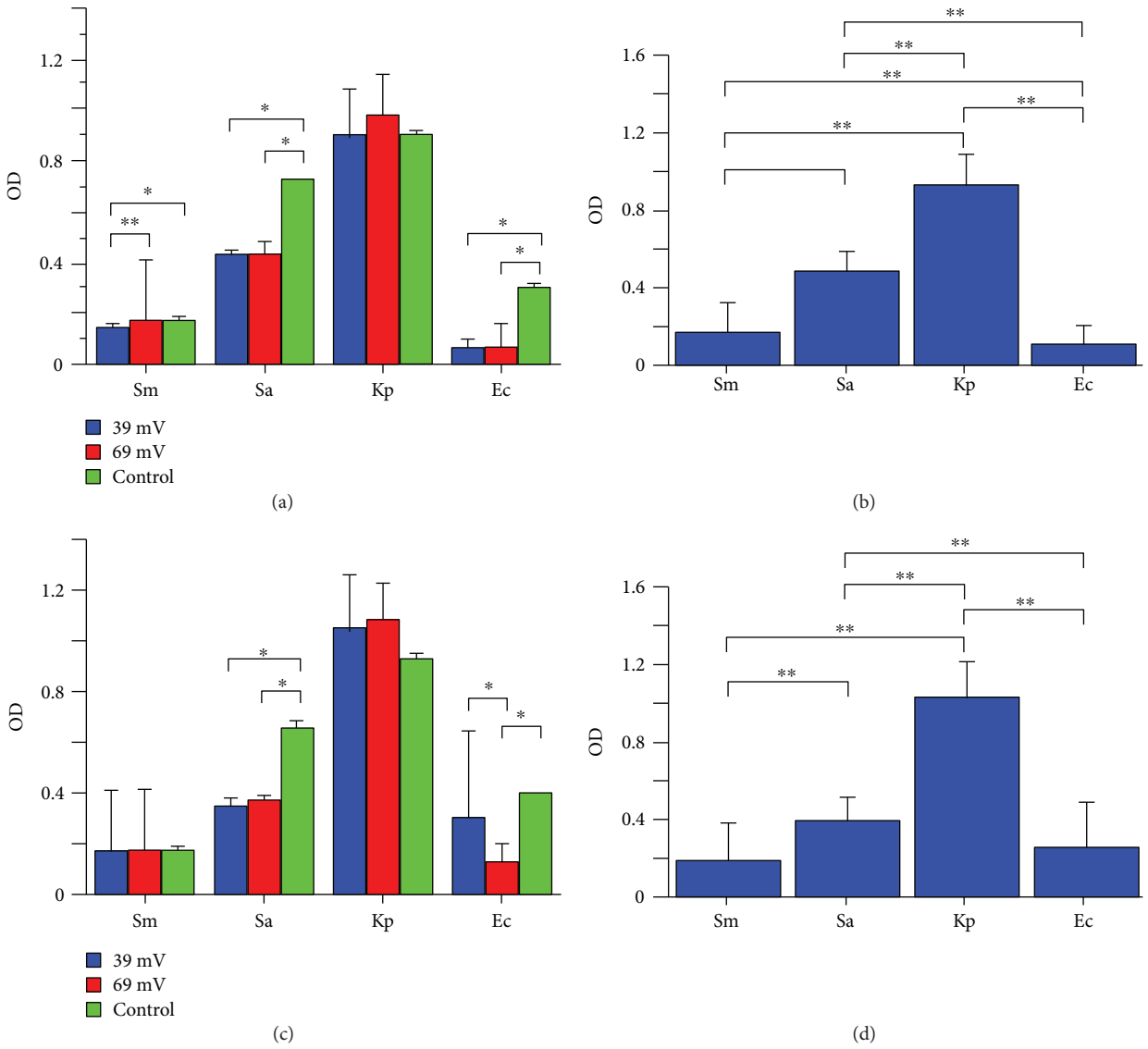

Figure 9: Bacterial sensitivity to AgP-alumina spheres treated at 24 and 48 h. (a) AgP-AS at 24 h for each voltage and microorganism. (b) General inhibition activity of AgP-AS at 24 h. (c) AgP-AS at 48 h for each voltage and microorganism. (d) General inhibition activity of AgP-AS at 48 h. $^{*}p < 0.05$; $^{**}p < 0.01$.

particles. In this sense, it is considered stable when the electrical charge is greater than 30 mV or −30 mV; conditions within this range will be probably agglomerated [28]. Thus, nonagglomerated particles could promote better antimicrobial activity compared to agglomerated nanoparticles increasing its superficial area producing higher contact zones on the bacterial cell [17, 18, 22]. Although this study did not evaluate the zeta potential of the Ag alumina samples and AgP-AS samples, it is very possible that electrostatic interactions between Ag particles and the negatively charged cell surface could bind and disrupt the cytoplasmic membrane of bacteria leading to damage of membrane functions, penetrating inside cells and inhibiting the vital metabolic process for cell survival [18, 22, 29, 30]. In the biomedical field, studies have already incorporated AgNPs into various medical devices and determined their antimicrobial activity against a wide variety of bacterial species concluding that these biomedical appliances with AgNPs could have a high potential of application to combat different types of bacterial biofilm decreasing the incidence or prevalence of those diseases considered serious health problems [31–34].

4. Conclusions

The optimal alumina-PVA ratio was 60 : 2, because it allows the preparation of a round material with sphericity of 1.02, and through electrodeposition, the doping with silver nanoparticles was achieved. The antibacterial effect against *S. aureus*, *E. coli*, and *S. mutans* was observed. Moreover, the effect of silver nanoparticles deposited on the surface of alumina spheres. Bacterial growth was not affected by pure alumina sphere; however, the presence and concentration of AgNPs determined gradually the antimicrobial activity on the different bacterial strains, even in lower silver

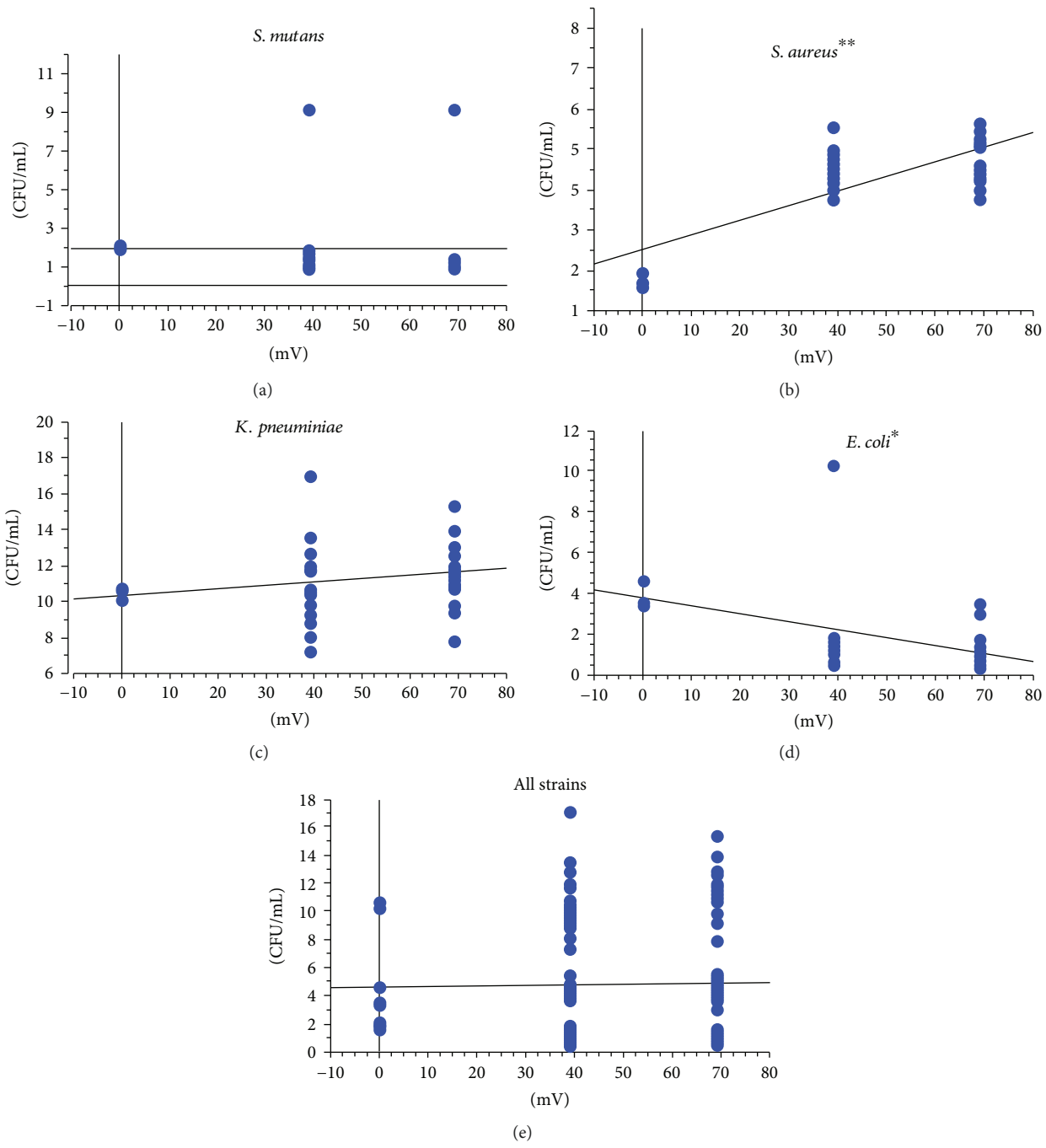

Figure 10: Pearson's correlation analysis. $^{*}p < 0.01$; $^{**}p < 0.001$.

electrodepositions. Also, Gram-negative bacteria demonstrated to be more sensitive Ag composites than Gram-positive strains, determining a dose-dependent activity. Alumina spheres doped with silver nanoparticles by electrodeposition technique demonstrated to have a high potential for biomedical applications.

Data Availability

The data used to support the findings of this study are available from the corresponding author upon request.

Conflicts of Interest

The authors declare that there is no conflict of interest regarding the publication of this paper.

Acknowledgments

The authors gratefully acknowledge the financial support by CONACYT and PROMEP. Simón Yobanny Reyes-Lopez thanks Dr. Carlos Rodriguez for SEM images.

References

[1] J. López-Esparza, L. F. Espinosa-Cristóbal, A. Donohue-Cornejo, and S. Y. Reyes-López, "Antimicrobial activity of silver nanoparticles in polycaprolactone nanofibers against gram-positive and gram-negative bacteria," *Industrial and Engineering Chemistry Research*, vol. 55, no. 49, pp. 12532–12538, 2016.

[2] C. S. Ciobanu, S. L. Iconaru, M. C. Chifiriuc, A. Costescu, P. le Coustumer, and D. Predoi, "Synthesis and antimicrobial activity of silver-doped hydroxyapatite nanoparticles," *BioMed Research International*, vol. 2013, Article ID 916218, 10 pages, 2013.

[3] R. Morones-Ramírez, "Historia de la plata: su impacto en las antiguas civilizaciones y la sociedad moderna," *Revista Digital Universitaria*, vol. 11, pp. 3–9, 2010.

[4] M. Rai, A. Yadav, and A. Gade, "Silver nanoparticles as a new generation of antimicrobials," *Biotechnology Advances*, vol. 27, no. 1, pp. 76–83, 2009.

[5] P. N. Quiroga, "Evaluación del potencial tóxico del proteinato débil de plata," *Acta Toxicológica Argentina*, vol. 19, pp. 85-86, 2011.

[6] N. V. Ayala-Núñez, *Nanopartículas de Plata Como Microbicidas: Actividad y Mecanismos de Acción Contra la Infección por el Virus de Inmunodeficiencia Humana (VIH) y Diferentes Cacterias Resistentes a Antibióticos. Doctoral Thesis*, Universidad Autónoma de Nuevo León, 2010.

[7] O. Choi, K. K. Deng, N. J. Kim, L. Ross Jr, R. Y. Surampalli, and Z. Hu, "The inhibitory effects of silver nanoparticles, silver ions, and silver chloride colloids on microbial growth," *Water Research*, vol. 42, no. 12, pp. 3066–3074, 2008.

[8] D. J. Paredes-Guerrero, *Estudio del Efecto Antibacteriano de Nanopartículas de Plata Sobre Escherichia coli y Staphylococcus aureus. Thesis*, Universidad Industrial de Santander, 2011.

[9] M. A. Laredo-Naranjo, *Propiedades Antimicrobianas y Cito-Toxicidad de las Nanopartículas de Plata Depositadas en Placas de Titanio In Vitro Master's Degree Thesis*, Universidad Autónoma de Nuevo León, 2014.

[10] G. G. Leyva, "Nanopartículas de plata: tecnología para su obtención, caracterización y actividad biológica," *Investigación en Discapacidad*, vol. 2, pp. 18–22, 2013.

[11] S. Y. Reyes-López, R. S. Acuña, R. López-Juárez, and J. S. Rodríguez, "Analysis of the phase transformation of aluminum formate $Al(O_2CH)_3$ to α-alumina by Raman and infrared spectroscopy," *Journal of Ceramic Processing Research*, vol. 14, pp. 627–631, 2013.

[12] J. H. Roque Ruiz and S. Y. Reyes Lopez, "Synthesis of α-Al_2O_3 nanopowders at low temperature from aluminum formate by combustion process," *Journal of Material Sciences & Engineering*, vol. 05, no. 6, pp. 1–8, 2016.

[13] C. J. E. Santos, T. S. Wei, B. Cho, and W. M. Kriven, "A forming technique to produce spherical ceramic beads using sodium alginate as a precursor binder phase," *Journal of the American Ceramic Society*, vol. 96, no. 11, pp. 3379–3388, 2013.

[14] B. Rezaei and S. Damiri, "Electrodeposited silver nanodendrites electrode with strongly enhanced electrocatalytic activity," *Talanta*, vol. 83, no. 1, pp. 197–204, 2010.

[15] K. A. Plonka, M. L. Pukallus, A. G. Barnett, L. J. Walsh, T. H. Holcombe, and W. K. Seow, "Mutans streptococci and lactobacilli colonization in predentate children from the neonatal period to seven months of age," *Caries Research*, vol. 46, no. 3, pp. 213–220, 2012.

[16] P. Moreillon and Y. A. Que, "Infective endocarditis," *The Lancet*, vol. 363, no. 9403, pp. 139–149, 2004.

[17] L. F. Espinosa-Cristóbal, G. A. Martínez-Castañón, R. E. Martínez-Martínez et al., "Antibacterial effect of silver nanoparticles against Streptococcus mutans," *Materials Letters*, vol. 63, no. 29, pp. 2603–2606, 2009.

[18] Á. M. Martínez-Robles, J. P. Loyola-Rodríguez, N. V. Zavala-Alonso et al., "Antimicrobial properties of biofunctionalized silver nanoparticles on clinical isolates of *Streptococcus mutans* and its serotypes," *Nanomaterials*, vol. 6, no. 7, p. 136, 2016.

[19] S. B. Bhardwaj, M. Mehta, and K. Gauba, "Nanotechnology: role in dental biofilms," *Indian Journal of Dental Research*, vol. 20, no. 4, pp. 511–513, 2009.

[20] R. Pena-Miller, D. Laehnemann, G. Jansen et al., "When the most potent combination of antibiotics selects for the greatest bacterial load: the smile-frown transition," *PLoS Biology*, vol. 11, no. 4, article e1001540, 2013.

[21] P. C. Appelbaum, "The emergence of vancomycin-intermediate and vancomycin-resistant *Staphylococcus aureus*," *Clinical Microbiology and Infection*, vol. 12, Supplement 1, pp. 16–23, 2006.

[22] L. F. Espinosa-Cristóbal, G. A. Martínez-Castañón, J. P. Loyola-Rodríguez et al., "Bovine serum albumin and chitosan coated silver nanoparticles and its antimicrobial activity against oral and nonoral bacteria," *Journal of Nanomaterials*, vol. 2015, Article ID 420853, 9 pages, 2015.

[23] M. K. Paczosa and J. Mecsas, "*Klebsiella pneumoniae*: going on the offense with a strong defense," *Microbiology and Molecular Biology Reviews*, vol. 80, no. 3, pp. 629–661, 2016.

[24] S. Chhibber, V. S. Gondil Gondil, S. Sharma, M. Kumar, N. Wangoo, and R. K. Sharma, "A novel approach for combating *Klebsiella pneumoniae* biofilm using histidine functionalized silver nanoparticles," *Frontiers in Microbiology*, vol. 8, p. 1104, 2017.

[25] T. V. Mathew and S. Kuriakose, "Studies on the antimicrobial properties of colloidal silver nanoparticles stabilized by bovine serum albumin," *Colloids and Surfaces. B, Biointerfaces*, vol. 101, pp. 14–18, 2013.

[26] Q. L. Feng, J. Wu, G. Q. Chen, F. Z. Cui, T. N. Kim, and J. O. Kim, "A mechanistic study of the antibacterial effect of silver ions on *Escherichia coli* and *Staphylococcus aureus*," *Journal of Biomedical Materials Research*, vol. 52, no. 4, pp. 662–668, 2000.

[27] E. Pazos-Ortiz, J. H. Roque-Ruiz, E. A. Hinojos-Márquez et al., "Dose-dependent antimicrobial activity of silver nanoparticles on polycaprolactone fibers against Gram-positive and Gram-negative bacteria," *Journal of Nanomaterials*, vol. 2017, Article ID 4752314, 9 pages, 2017.

[28] J. M. Ibarra-Hurtado, A. Virgen-Ortiz, A. Apolinar-Iribe, and A. Luna-Velasco, "Control and stabilization of silver nanoparticles size using polyvinylpyrrolidone at room temperature," *Digest Journal of Nanomaterials and Biostructures*, vol. 9, no. 2, pp. 493–501, 2014.

[29] L. Treuel, S. Brandholt, P. Maffre, S. Wiegele, L. Shang, and G. U. Nienhaus, "Impact of protein modification on the protein corona on nanoparticles and nanoparticle-cell interactions," *ACS Nano*, vol. 8, no. 1, pp. 503–513, 2013.

[30] W. Lee, K. J. Kim, and D. G. Lee, "A novel mechanism for the antibacterial effect of silver nanoparticles on *Escherichia coli*," *Biometals*, vol. 27, no. 6, pp. 1191–1201, 2014.

[31] A. E. Hernández-Gómora, E. Lara-Carrillo, J. B. Robles-Navarro et al., "Biosynthesis of silver nanoparticles on orthodontic elastomeric modules: evaluation of mechanical and antibacterial properties," *Molecules*, vol. 22, no. 9, 2017.

[32] G. Metin-Gürsoy, L. Taner, and G. Akca, "Nanosilver coated orthodontic brackets: *in vivo* antibacterial properties and ion release," *European Journal of Orthodontics*, vol. 39, no. 1, pp. 9–16, 2017.

[33] A. R. Mhaske, P. C. Shetty, N. S. Bhat et al., "Antiadherent and antibacterial properties of stainless steel and NiTi orthodontic wires coated with silver against *Lactobacillus acidophilus*—an in vitro study," *Progress in Orthodontics*, vol. 16, no. 1, article 40, 2015.

[34] J. Y. Choi, C. J. Chung, K. T. Oh, Y. J. Choi, and K. H. Kim, "Photocatalytic antibacterial effect of TiO_2 film of TiAg on *Streptococcus mutans*," *The Angle Orthodontist*, vol. 79, no. 3, pp. 528–532, 2009.